Journal of Geodynamics 121 (2018) 9–19

Contents lists available at ScienceDirect

Journal of Geodynamics

journal homepage: www.elsevier.com/locate/jog

Post-Deccan Trap stress reorientation under transpression: Evidence from fault slip analyses from SW Saurashtra, Western India

Naimisha Vanik[a], Mohamedharoon A. Shaikh[a], Soumyajit Mukherjee[b], D.M. Maurya[a,*], L.S. Chamyal[a]

[a] Department of Geology, The Maharaja Sayajirao University of Baroda, Vadodara, 390 002, Gujarat, India
[b] Department of Earth Sciences, Indian Institute of Technology Bombay, Powai, Mumbai, 400 076, Maharashtra, India

ARTICLE INFO

Keywords:
Stress analyses
Brittle shear zones
Indian tectonics
Shear zone analyses
Deccan trap
Saurashtra, Western India

ABSTRACT

We analyze paleostress from a region in SW Saurashtra (India) using three free software, T-Tecto, WinTensor and FaultKin based on attitudes of ~ E-W trending, sub-vertical, brittle fault planes and associated horizontal, inclined and subvertical slickensides, developed over them. We present a detailed fault slip analysis of a previously unmapped E trending fault (herein referred as the Katar Fault) that cuts across and offset the southeastward dipping Deccan lava flows with a dense NE-SW trending dyke swarm belonging to Deccan Trap near Rajula (Gujarat, India). Measured fault strikes do not match exactly with ~ NW/NNW trending basement structures, deduced by previous geophysical studies, nor with faults reported from the offshore Saurashtra region. However, a few geomorphic features around Katar indicate a similar strike slip offset. A stress ratio of up to 0.2, and a SE maximum principal stress axis were deduced using T-Tecto, while WinTensor and FaultKin gave plunging stress axes. Therefore, stress analyses by T-Tecto seem more plausible. The SH_{max} direction usually remains close to one of the stress axes, and shows up to 36° rotation when compared with the offshore region. We attribute the formation of Katar Fault to post-Deccan Trap oblique slip reverse faulting with sinistral slip due to intraplate transpressional stresses induced by the anticlockwise rotation and collision of the Indian plate with the Eurasian plate at ~ 55 Ma. This transpressional faulting post-dates the eastward tilting of lava flows and anticlockwise rotation in the dyke swarm patterns caused by the emplacement of large Girnar intrusive body. Detailed structural geological field-work in Saurashtra would be much required to understand its onshore tectonics.

1. Introduction

Paleostress analyses, using fault planes and associated slickenlines attitudes, is extremely useful in deciphering regional tectonics, especially in finding trends of the stress axes (e.g., Kaymakci, 2006; Zalohar, 2018; Simón, J. L. (In Press)). When integrated with either new or already existing nearby offshore geophysical data, such works turn out to be more fruitful (e.g., van Gent et al., 2009; Misra et al., 2015). A number of free software with in-built statistical algorithm have been available to perform paleostress analyses based on field-acquired structural data.

How stresses could have acted inside the Deccan trap in Saurashtra remained so far indeterminate due to *(i)* paucity of structural geological field-studies from this terrain; and *(ii)* lack of absolute dates/durations of faulting of some of the nearby fault planes in mega-scale. The offshore region of Saurashtra being a frontier area for petroleum exploration (Directorate General of Hydrocarbons, DGH), hence, paleostress studies around this region can have far reaching implication in well-bore stability studies.

Having generated a fault plane and slickenside database around Rajula (southern Saurashtra, India), this work analyses paleostress of an E-W trending fault. The vicinity of the study site is characterized by numerous parallel NE trending dykes The trend of the dyke swarm suggests rotation of structural trend as these are found to be trending in E-W direction ~ 20 km NE of the study area (Chatterjee and Bhattacharji, 2001). The E-W trending Katar Fault cuts across these dyke ridges and appears to be a purely strike-slip fault in the first instance as it offsets the ~ 65 Ma trappean lava flows which are tilted towards south east. The fault has not been mapped previously, and in fact no tectonic map of the region around Rajula exists till date. The main objective of this study is to precisely delineate the slip characteristics of the fault and explore its possible implication on tectonic set up of the area.

* Corresponding author.
E-mail address: dmmaurya@yahoo.com (D.M. Maurya).

https://doi.org/10.1016/j.jog.2018.06.004
Received 7 September 2017; Received in revised form 9 May 2018; Accepted 17 June 2018
Available online 24 June 2018
0264-3707/

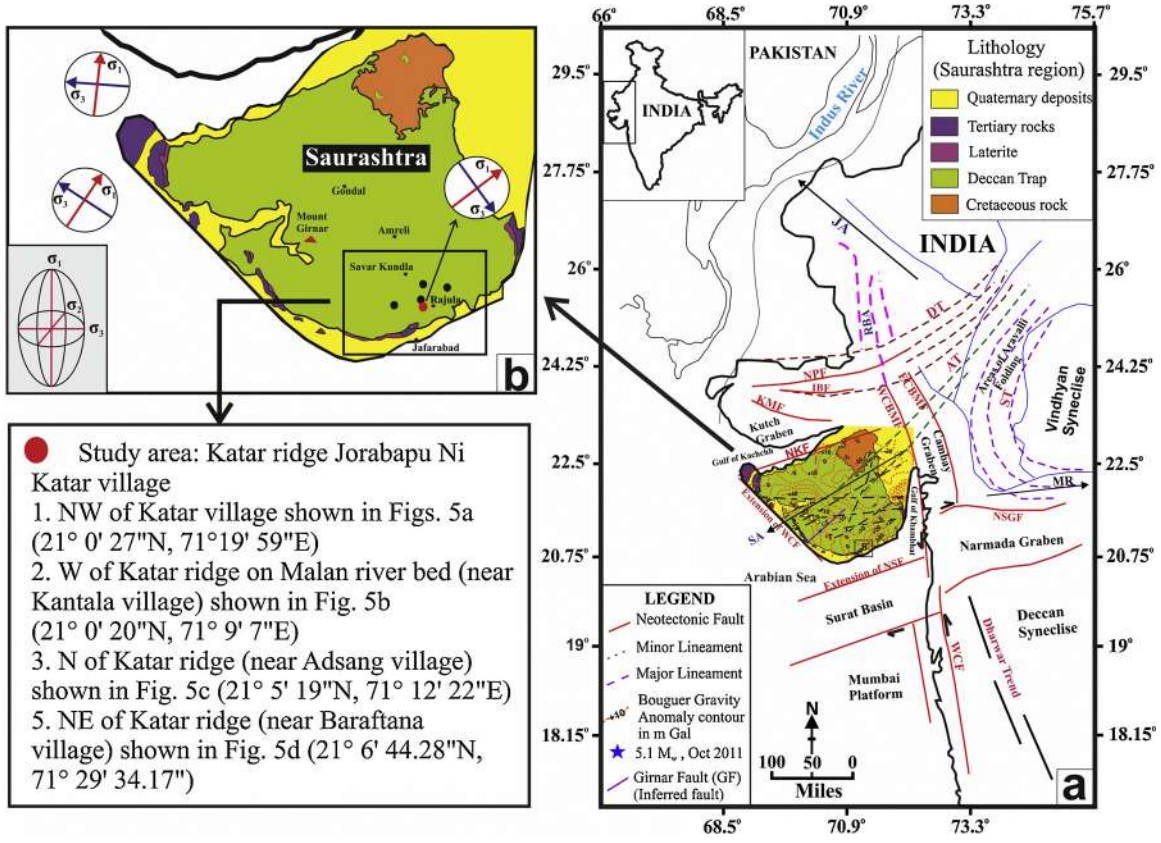

Fig. 1. a) Tectonic map of Gujarat that represents major and minor structural lineaments, peri-cratonic rift basins, gravity anomaly and major faults. Pink, green and maroon dotted lines: ST- Satpura Trend, AT- Aravalli Trend, and DT- Delhi Trend, respectively. Red line: major regional faults: IBF-Island Belt Fault, NPF- Nagar Parker Fault, KMF- Kutch Mainland Fault, WCF- West Coast Fault, WCBMF- Western Cambay Basin Margin Fault, ECBMF- Eastern Cambay Basin Margin Fault, NSF-Narmada Son fault, NSGF- Narmada Son Geofracture. JA- Jaisalmer Arch, SA- Saurashtra Arch, RBA-Radhanpur Barmer Arch, MR- Malwa Ridge are the tectonic regional arch and ridges surrounding Saurashtra peninsula. Blue star: M_w 5.1 earthquake on Oct 2011 near Talala (T). Pink line: inferred causative Girnar Fault (GF) based on deep seismic profiles and gravity studies. (For interpretation of the references to colour in this figure legend, the reader is referred to the web version of this article).

Compiled and modified from Biswas (1987); Merh (1995); Dasgupta et al., (2000) and Rastogi et al., (2013). Several other lineaments with varying structural trends are mapped by Bhattacharya et al., (2004) in SW Saurashtra region. (b) Map of the Saurashtra region showing study area and the surrounding regions at S and SE. Red circle: Study area (near Katar village), black circles: areas surrounding the study area. Red triangle: Mount Girnar. Left down corner shows prolate stress ellipsoid (detail in Section 4). Stress directions obtained from Kachchh and Saurashtra offshore basin (Kundan et al., 2017) and from our study area (Katar ridge fault).

2. Geology & tectonics

Mainly Mesozoic and Cenozoic rocks crop out in the Saurashtra peninsula (southern Gujarat, India; Fig. 1). The oldest rock comprise Upper Jurassic sedimentary sequence exposed in the northeastern part followed by multiple flows of Deccan Trap Formation within most part of the Saurashtra peninsula (Merh, 1995). The Cenozoic sequence consisting of Tertiary and Quaternary sediments occur along the coastal zone fringing the Deccan flows (Dasgupta et al., 2000).

The Girnar hill is a large laccolithic intrusive that covers ~ 173.53 km^2, and is located ~ 95 km NW of the study area (Fig. 1). The intrusive mass, which also forms the highest elevation in Saurashtra, comprises of differentiated igneous complex consisting of olivine gabbro, biotite-diorite, monzonite, nepheline syenite, granophyre, quartz felsite along with dykes of feldspar and quartz-feldspar (Mathur et al., 1926; Verma and Mittal, 1972; Paul et al., 1977). The intrusion postdates Deccan Trap time at 64.1 ± 1.4 my (Wellman and McElhinny, 1970).

The Saurashtra region is an uplifted mass of WSW plunging basement arch, which distributes the western continental margin into a "Kutch-Saurashtra shelf" and a southern "Mumbai-Kerala shelf" (Biswas, 1987). The block is bound by three major Precambrian rift trends viz., the Delhi-Aravalli trend (NE), the Son-Narmada trend (ENE) and the Dharwar trend (NNW; Repository Fig. 1). The interplay of these three Precambrian basement framework characterizes the structural architecture of the region (Biswas, 1987). The region is also surrounded by major faults viz., North Kathiawar Fault (NKF) at N, extension of West Coast Fault (WCF) at W, extension of the Narmada-Son Fault (NSF) at S and Western Cambay Basin Margin Fault (WCBMF) at E (Fig. 1).

The North Kathiawar Fault (NKF), at the northern margin of the Saurashtra region, is a ~ NW trending normal fault formed during Early Jurassic or earlier along with Kutch basin and lower Narmada-Tapti valleys (Gowd et al., 1996). During Cretaceous-Paleocene, the Saurashtra block parted by repeated slips along the western extension of Great Boundary Fault (GBF) forming the NKF (Biswas, 1987). The ~NE Aravalli trend continues across the Cambay graben into Saurashtra forming SW plunging Saurashtra Arch (Dasgupta et al., 2000). The northward extension of Dharwar trend to the W part of the Indian shield through the Narmada rift produced Cambay/Khambat graben (Biswas, 1987). This graben to the E is intracratonic, bound by the Radhanpur-Barmer Arch at W and Aravalli belt at E (Bastia and Radhakrishna, 2012). The Eastern Cambay Basin Margin Fault (ECBMF) at E and the Western Cambay Basin Margin Fault (WCBMF) at W confine the Cambay graben (Fig. 2a). The WCBMF trends NNW east to Bhavnagar (Saurashtra region) and is associated with several low to moderate magnitude earthquakes (Yadav et al., 2008; Rastogi et al., 2013). The E-W trending Shihor Fault cuts the WCBMF trending N-S

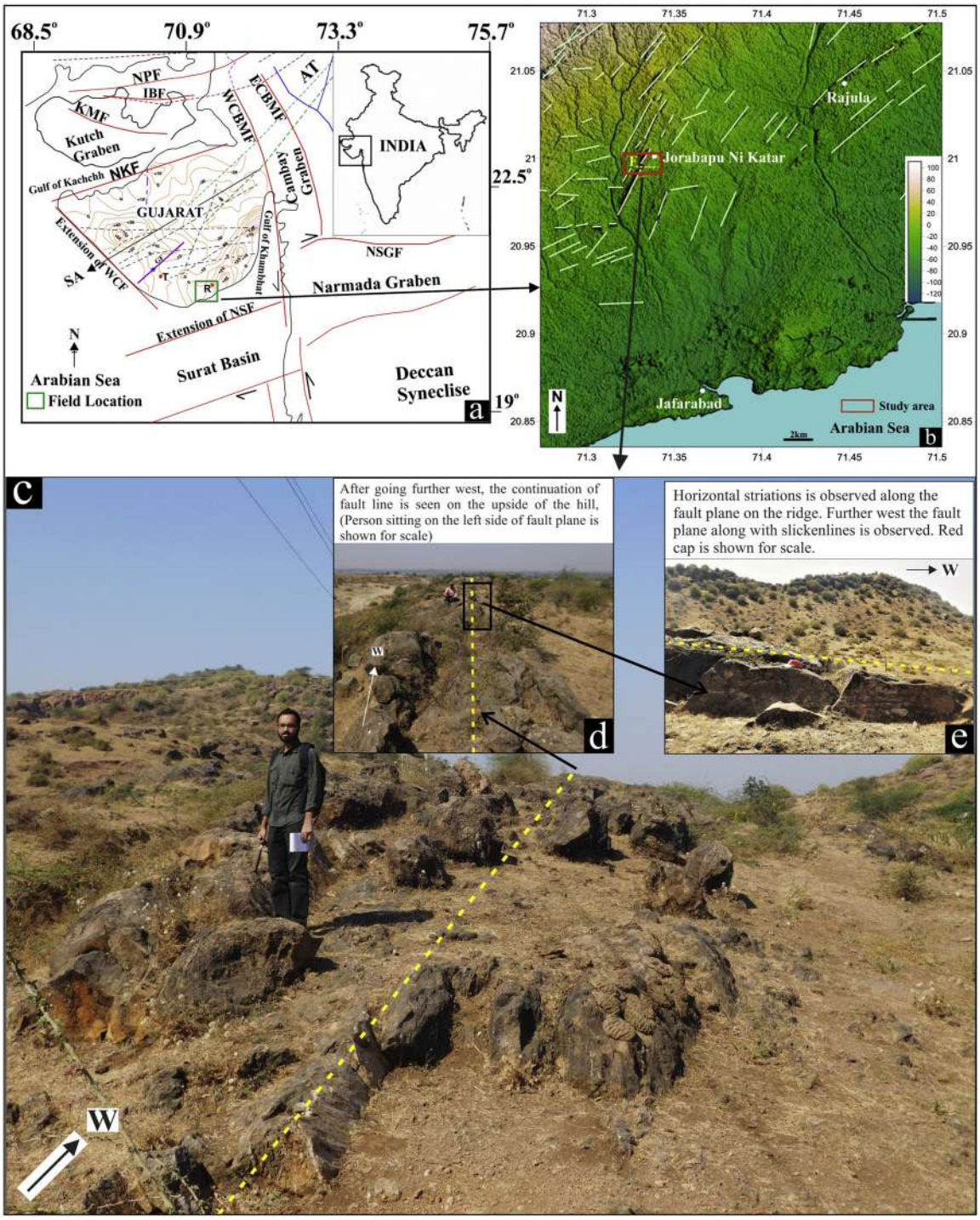

Fig. 2. a) Study area shown within green box in tectonic map of Gujarat. R: Rajula town. (b) DEM of the area: prominent NNW trending ridges surround Rajula. Red box: E trending fault ~ 1 km cutting NW trending ridge W to "Katar" village. (c) Meso-scale fault cuts the Katar Ridge exposed near the "Katar" village W to Rajula. Yellow dotted line: fault plane. Height of the person is 175 cm as scale. The fault line continues further towards W, as in photo. (d) These fault planes show different types of striations: such as horizontal in photo (e) Red cap as scale. The E trending fault cutting the NW trending ridge shows such slickensides. (For interpretation of the references to colour in this figure legend, the reader is referred to the web version of this article).

near Bhavnagar (E Saurashtra) is responsible for earthquake swarm activities in this region (Bhattacharya et al., 2004). The basin separated from the Bombay/Mumbai offshore basin at S (Fig. 2a) by the seaward extension of Narmada-Son Fault (NSF; Chamyal et al., 2002; Joshi et al., 2013; review in Valdiya, 2016). The extension of the NSF also continues in the Arabian Sea and across the Saurashtra continental margin (Bhattacharya and Subrahmanyam, 1986).

The westward lineament extension as dyke swarms at SE part of Saurashtra are mainly aligned (sub)parallel to the major tectonic grains (Fig. 2b). The dykes swarms observed in the S and SE area of Saurashtra associated with the Deccan volcanism cluster along E trending Narmada-Son-Tapti/Tapi belt (review: Mahadevan, 1994). Countless prolific dykes are massive and resistant to erosion and form prominent positive relief in Saurashtra (Mishra, 2008; Dasgupta, 2018).

The Landsat data of the peninsular coastal India shows three major lineament trends viz., NE, NW and ENE relates to Dharwar, Eastern

Ghat and Satpura in central India, respectively. The Dharwar trend is the oldest whereas Satpura trend is the youngest (Biswas, 1987; review in Varadarajan and Ganju, 1989). LANDSAT-1 imagery and aerial photographs of the SE Saurashtra region decode dense NE, NNW and NW lineaments depicting the extension of Narmada-Son lineament (Ramasamy, 1995). Horizontal E-W compression affected Saurashtra tectonically (Ramasamy, 1995).

Chatterjee and Bhattacharji (2001, 2004) studied geochemistry and geochronology of SE Saurashtra and inferred that the ~ 65 Ma age of the Rajula felsic rocks is equivalent to the Deccan Volcanics. Chatterjee and Bhattacharji (2004) did a preliminary geochemical study of zircon and monazite of Deccan felsic dykes near Rajula (Amreli, Saurashtra). Their study indicates the maximum crustal heating of approximately 900° C due to Deccan trap lava intrusion and 1–2 Ma settling time over the Pre-Deccan trap dykes. The Rajula area and its surroundings is crossed by E, ENE, WSW dyke swarms that trend NW towards W (Fig. 2b).

Deep seismic sounding profiles (DSSP) crossing Amreli, ~ 67 km N of Rajula did not reveal noteworthy structures which could be due to the resolution of the data, and low impedance contrast across the fault plane, since the faults juxtapose the same lithology. However, integrated geophysical studies indicated that the (sub)basement structures trend NNW (Reddy, 2005). The Bouger gravity anomaly observed along the NE trending region: Amreli-Rajkot-Surendranagar is low (~ 30 mGal), which is skirted by gravity high zones. The Bouger anomaly contours around Rajula area shows gravity high zones (~ + 30 to + 40 mGal) over linear dykes trending ENE to E and plugs. Three circular highs of ~ same amplitude is observed SE part of the Saurashtra connected with NE oriented structural trend that indicates deep-seated faults/fracture zones (Chandrasekhar et al., 2002).

The Rajula region comes under the zone III in the isoseismal map of earthquake at the Saurashtra coast. This approximately elliptical isoseismal zone trends NE (Dasgupta et al., 2000). The Rajula area also experienced ≥5 magnitude offshore earthquakes in August 1986 and September 1993 (Yadav et al., 2011; Rastogi et al., 2013). But there is no report of any faults/tectonic activity linked with the minor shocks. However, the Talala region ~ 100 km W to Rajula and the nearby regions experienced significant shocks since 2001 (Yadav et al., 2011). Yadav et al.'s (2011) fault plane solution revealed steeply-dipping NE striking vertical faults to be responsible for the ongoing shocks. GPR studies by Bhatt et al., (2006) confirmed faults at shallow-depth around the Katar ridge.

3. Field studies

We studied faults in field in detail *(i)* over a ~ E trending ~ 1 km long ridge W to the Katar village near the Rajula town, South Saurashtra; and at selected locations *(ii)* around Katar. The Katar ridge was first selected using the Google Earth image along with the Survey of India topographical maps. We identify E trending ~ vertical fault planes based either on prominent striation-bearing fault planes (Figs. 2c–e), or by noting P-planes ~ perpendicular to those fault planes, i.e., on ~ horizontal planes. Three categories of striations were noted: horizontal, vertical and oblique (Figs. 3 a–d). At few places, P- and Y- brittle shear planes were observed where the sigmoid P-planes merge ~ tangentially with the Y-planes indicating sinistral- (Figs. 3e–g). These are considered reliable slip sense indicators (e.g., Means, 1987; Mukherjee and Koyi, 2010; Mukherjee, 2013, 2014, 2015a,b; Misra et al., 2014; Dasgupta and Mukherjee, 2017; Misra and Mukherjee, 2017).

Slickenside striations with kinematic indicators like fractures perpendicular to the fault surface in the direction of movement have been observed on the megascopic-scale to identify the slip sense (Fig. 3a–d). Sigmoid tension gashes, hybrid fractures and step-like indicators as slickolite markers (Doblas, 1998) were observed on the fault planes (Fig. 3a and c). Most of the horizontal slickenside striations indicate dextral slip. Few other (sub)horizontal striations with shear sense indicators are also observed (Repository Fig. 2). Which faulted block exactly moved up or down was difficult to decipher from most of the vertical striations (Fig. 3b) since they are indistinct kinematic indicators. However, features related to contraction like broken edges and arrow-shaped micro-gouges on the fault plane are identified as reliable kinematic indicators (Fig. 3b). Several other cases of (sub)vertical to oblique striations were observed (Repository Fig. 3).

The steps or peaks face upslope indicating the slip sense (Fig. 3c). Asymmetric curved elevations, peaks and step like features on the rock surface have been observed in oblique striated planes (Fig. 3c). Depending on the friction between the slipping fault blocks, the orientation of steps rises towards the motion of the opposite block. Some more well-developed inclined/oblique striations observed (Repository Fig. 4). In few cases we deciphered the slip sense by moving hand softly parallel to the slickensides to know the positive and negative smoothness criterion i.e., finding out the direction of smoothness (Doblas et al., 1997, 1998).

Oblique striations mostly indicate reverse faulting (Fig. 3c) and in few cases normal faulting (Repository Fig. 4e and f). Few of the E trending faults show very poorly developed slickensides with ambiguous slip sense (Fig. 3d, Repository Fig. 5). The sense of shear at these sub-vertical fault planes appears to be either horizontal (i.e. strike-slip) or oblique (i.e., oblique-slip). In one of the sub-vertical fault planes, two different trends of oblique striations have also been observed (Fig. 3h).

4. Fault slip analyses

Paleostress analyses was performed on the collected fault-slip data to derive the stress tensors for the Katar Fault. The fault-slip data includes fault plane orientation, sense of slip (normal/reverse/dextral/sinistral) and slickenside orientation. A total of 46 fault-slip data (attitudes of fault planes and slickensides) was used for fault slip analyses, using T-Tecto Studio X5, Win-Tensor (v5.8.7) and FaultKin (v7.7.2) (Appendix A for working principles). These paleostress inversion software have been developed based on the assumption that the observed slip direction is parallel to the maximum resolved shear stress on the fault plane (Bott, 1959; Wallace, 1951). The sense of movement along a fault plane is derived from one stress tensor that has been active during a certain period. Therefore, it is necessary to divide the heterogeneous fault-slip data into homogeneous subsets so as to determine paleostress state of the particular deformation event (Kounov et al., 2011). Homogeneous subset of data are those that are produced by a single deformation phase. The field photograph shows cross-cutting relationship of two oblique slip striations and therefore it was difficult to determine the homogeneous subsets based on the striae superimposition criteria (Fig. 4a and b).

In such a scenario, separation of the heterogeneous fault-slip data was performed using T-Tecto software. The software separated the heterogeneous fault-slip data into homogeneous subsets of Phase 1 (Fig. 4c) and Phase 2 (Fig. 4d) by using the Gauss weighted right dihedra method (RDM). The Gauss method sort out the heterogeneous fault slip data into the homogeneous fault subsystems (Zalohar and Vrabec, 2007) and the RDM (Angelier, 1989, 1990) calculates the stress tensor of each homogeneous fault subsystems. Fig. 4 and Tables 1 present the results. The phase 1 shows that maximum compressive stress (σ_1) is N315° E and 94% of the fault set data represents this stress trend (Fig. 4c). While phase 2 shows that the maximum compressive stress (σ_1) is N53° E and 99% of the fault set data represents this trend (Fig. 4d). Hence, the two deformation phases show entirely different trend of maximum principal horizontal stress. T-Tecto deduced stress ratio [$R = (\sigma_2 - \sigma_3) \times (\sigma_1 - \sigma_3)^{-1}$] ranging 0–0.2. The transpressive stress regime has prevailed as shown by the stress ratio (R) of 0 and 0.2 in Phase 1 and Phase 2 deformation event respectively generated by T-Tecto software. The advantage of paleostress analyses is that, R can be deduced which indicates the shape of the stress ellipsoid even though

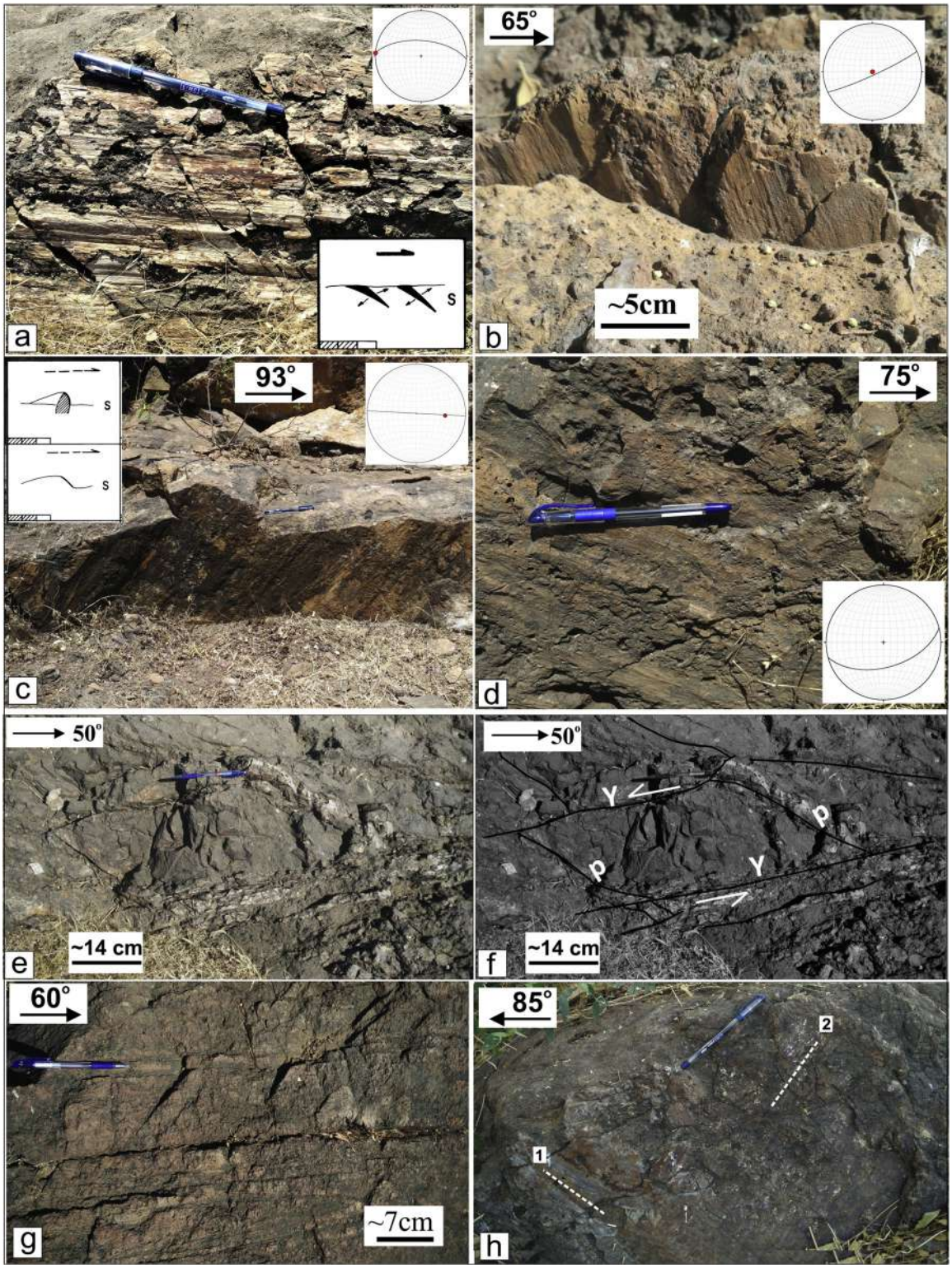

Fig. 3. Location: SW region of "Katar" village near Rajula. Inset: stereo-plot: great circle- fault, red dot- lineation. (a) Sub-vertical undulating fault plane (attitude: 93° strike, 62° dip, 3° dip direction) with horizontal striations. 14.3 cm long pen as scale. Fractures at high-angle to the fault. Inset: Fig. 1(FR) of Doblas et al. (1997). (b) Fault plane (attitude: 65° strike, 84° dip, 155° dip direction) with (sub)vertical striations. Damaged border and arrow-shaped micro-gouges define striation. Inset: Fig. 1 of Doblas et al. (1997). (c) Ridges and groove connoting oblique striations (rake 51°, trend 94°) on a fault plane (attitude: 93° strike, 90° dip, 3° dip direction). Slip sense indeterminate. 14.3 cm long pen as scale. (d) Very faint/poorly developed (sub)horizontal lineations on sub-vertical fault plane (attitude: 75° strike, 54° dip, 165° dip direction). Inset: stereo-plot of faults with ENE trend. 14.3 cm long blue pen as scale. Interpreted (e) and un-interpreted (f) photograph: P- and Y- brittle shear planes trend NE on a horizontal plane on a basaltic rock. The sigmoid P-plane merging the Y-plane show sinistral slip. (g) P- and Y- brittle shear planes on a horizontal basaltic rock surface showing dextral slip. (h) A curvi-planar fault plane with two trends of oblique striations. A 14.3 cm long blue pen as scale. At "1", fault plane attitude: 285° strike, 70° dip, 15° dip direction. Striation plunge: 53°, trend: 315°. At "2", fault plane attitude: 109° strike, 73° dip, 19° dip direction. Striation with plunge: 35°, trend: 95°. Note the overlapping of oblique striations at the bottom of the field photograph. (For interpretation of the references to colour in this figure legend, the reader is referred to the web version of this article).

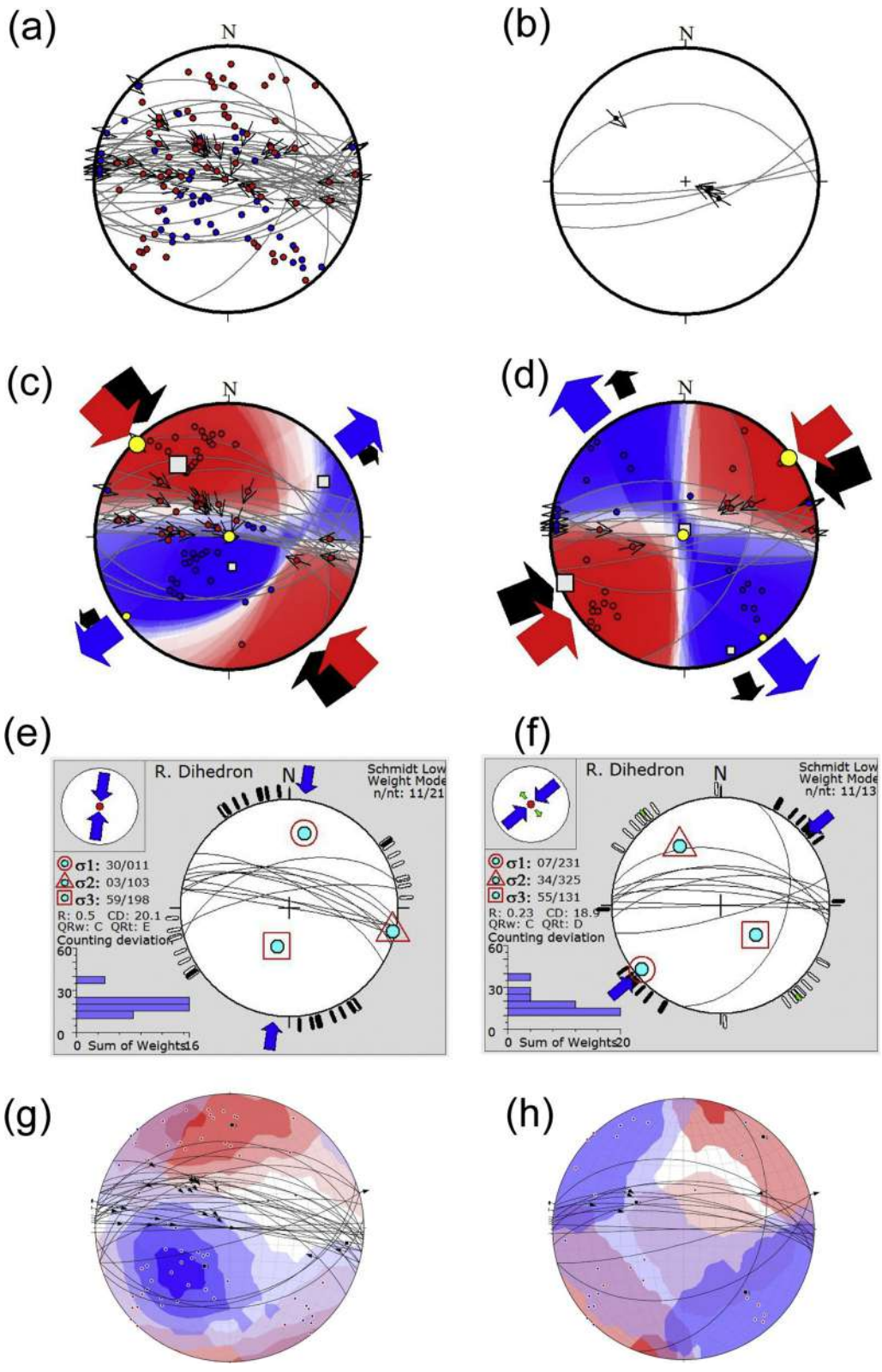

Fig. 4. Results of fault-slip inversion analysis performed for heterogeneous fault-slip data using T-Tecto, WinTensor and FaultKin software. (a) Stereo plot (lower hemisphere) - grey lines: fault planes with slip vectors marked by black dot with arrows. Red and blue dots: direction of P- (compressive) and T- (extension) kinematic axes for the individual fault plane respectively. (b) Stereo plot of fault planes misfit in the resultant tensor. (c) & (d) Resultant stress tensors of Phase 1 and Phase 2 deformation, respectively, generated from T-Tecto software. Squares: directions of principal stress axes obtained by the Gauss weighted Right Dihedra Method. Yellow circles: directions of principal strain axes by Visualization of Gauss Function method. Biggest square and yellow circle: direction of σ_1; Medium square and yellow circle: direction of σ_2; smallest square and yellow circle: direction of σ_3. Red inward- and blue outward arrows: direction of compressive and tensile stress, respectively. Red and blue quadrants of the graph: compressive and extensive strain fields, respectively. (e) & (f) show resultant stress tensor of Phase 1 and Phase 2 deformation generated from fault-slip inversion analysis for homogeneous subset of fault-slip data using WinTensor. Black lines: fault planes with slip vectors marked by open circles with arrows. Black solid lines and open lines at the periphery of the stereoplots: direction of SH_{max} and SH_{min} kinematic axes, respectively, for individual fault slip data. Stress symbol in the upper left corner. The orientation of the principal axes of the stress ellipsoid and the stress ratio (R) suggest the stress regime. The length and color of the horizontal stress axes (SH_{max} and SH_{min}) in the stress symbol: horizontal deviatoric stress magnitude (Delvaux et al., 1997). The vertical stress (σ_v) is indicated by a blue (σ_1) / green (σ_2) / red (σ_3) solid circle in the middle of the stress symbol suggesting the extensive/ strike-slip/ compressive stress regime. Stress tensors in the middle: blue inward arrows- compressional deviatoric stress ($SH_{max} = \sigma_1$); red outward arrows: tensile deviatoric stress. Circle, triangle and square: direction of maximum principal stress (σ_1), intermediate principal stress (σ_2) and minimum principal stress (σ_3), respectively. "n/nt": ratio of fault slip data used relative to the total number of fault slip data entered (Delvaux and Sperner, 2003). The graph of counting deviation is shown at the lower left corner of the graph. (g) and (h) show fault-slip inversion analysis performed for homogeneous subset of fault-slip data using FaultKin. Stereo plots of resultant stress tensors of Phase 1 and Phase 2 deformation are shown respectively. Black lines- fault planes with slip vectors marked by a black dot with arrows. Red and blue dots: directions of P- (compressive) kinematic axis and T- (extension) kinematic axis for the individual faults, respectively. Red and blue contours: compressive and tensile strain fields, respectively. Green squares: the direction of the principal stresses.

Table 1
Fault slip analysis performed with T-Tecto studio X5, Win-Tensor and FaultKin for *heterogeneous fault-slip data* (as in Delvaux and Sperner, 2003; Allmendinger et al., 2012). The results are given as homogeneous subsets divided in Phase 1 and Phase 2 deformation. n: number of fault-slip data used in the inversion. σ_1, σ_2 and σ_3: principal stress axes. Stress ratio $R = (\sigma_2 - \sigma_3) \times (\sigma_1 - \sigma_3)^{-1}$. Meaning of "Magnitude": for example for the underlined magnitude, 94% out of 23 fault data can be represented by 315° trend and 0° plunge.

Sl. no.	Software	n	Fault type	σ_1			σ_2			σ_3			Stress ratio R (unit less)	Stress regime as per Delvaux et al. (1997)
				Trend (in degrees)	Plunge (in degrees)	Magnitude	Trend (in degrees)	Plunge (in degrees)	Magnitude	Trend (in degrees)	Plunge (in degrees)	Magnitude		
Phase 1														
1	T-Tecto	23	Oblique slip reverse, sinistral slip	315	0	94%	82	89	N/A	232	0	82%	0.2	*Transpressive*
2	WinTensor	11	Oblique slip reverse, sinistral slip	11	30	–	103	3	N/A	198	59	–	0.5	*Pure compressive*
3	FaultKin	23	Oblique slip reverse, sinistral slip	220.5	51.7	–	78.2	32	N/A	336	18.7	–	–	–
Phase 2														
4	T-Tecto	14	Oblique slip reverse, sinistral slip	53	0	99%	292	90	N/A	142	0	96%	0	*Transpressive*
5	WinTensor	11	Oblique slip reverse, sinistral slip	231	7	–	325	34	N/A	131	55	–	0.23	*Transpressive*
6	FaultKin	14	Oblique slip reverse, sinistral slip	135.6	32.9	–	299.6	56	N/A	40.7	7.4	–	–	–

absolute stress magnitudes are indeterminate (Fossen, 2016). For example R = 0, as obtained for "oblique-slip reverse fault with sinistral slip" faults (Fig. 4, Table 1) indicates a prolate stress ellipsoid (Fig. 1). Since, all the R values are $< \ < 1$, none of the stress ellipsoids in these cases are oblate (uniaxial tension).

Fig. 4 and Table 1 avoided purely dip-slip normal- and reverse faults in the analyses. The separated homogeneous subsets of heterogeneous fault-slip data were then entered into WinTensor (Figs. 4e and f) and FaultKin (Figs. 4g and h) software. These were done in order to compare results obtained from T-Tecto, Win-Tensor and FaultKin (discussed later). Win-Tensor software aided to deduce the stress axes attitudes for fault types (Figs. 4e and f, Table 1) that can be compared with T-Tecto deductions (Figs. 4c and d, Table 1). For oblique-slip reverse fault with sinistral slip, attitude of the σ_1-axis is 315° (trend) and 0° (plunge) as per T-Tecto (Fig. 4c, Table 1), and 11° (trend) and 30° (plunge) as per Win-Tensor (Fig. 4e, Table 1).

Comparing fault-slip analyses results summarized in Table 1, one notes a wide mismatch of attitudes of stress axes for different fault types, such as sl 1, 2 and 3. As per Anderson's theory, two of the stress axes remain horizontal and the third one vertical. This constrain is more closely obeyed by the T-Tecto results (Figs. 4c and d, Table 1) than that by Win-Tensor (Figs. 4e and f, Table 1). Incompatible fault-slip data has not been considered in the resultant stress tensor. The compatibility of the data is determined through the right dihedral method (e.g., Betka et al., 2016). One limitation of FaultKin software is that it cannot provide the R value. Subsequently, it is not possible in this method to visualize the shape of the stress ellipsoid.

5. Discussion

5.1. Implication for stress scenario of SW Saurashtra

Extensional faults trending ~ E-W in Saurashtra would be expected since the terrain has been under an extensional stress before the Indian plate collided with the Eurasian plate ~ 55 Ma back (Mukherjee, 2015a,b). After the collision, compressive regime prevailed that produced NE, NW and ENE lineaments and fault sets in S to SW Saurashtra. These lineaments and fault sets of different major trends has been observed in Rajula and surrounding areas (Fig. 2b).The offshore region S of Rajula shows several inversion structures because of transpressional and transtensional strike-slip movement (Pandey et al., 2013). Around Rajula (< 60 km), most of the brittle shear planes show sinistral slip (Fig. 5, Repository Fig. 6–8) suggesting overall transpressional regime. Fig. 6 summarizes slip senses observed for such strike-slip shear.

Gowd et al., (1992) determined N23° E trend of the horizontal maximum compressive stress (SH_{max}) by borehole breakouts, hydrofracturing and focal mechanisms from the Indian peninsula. SH_{max} results are also obtained by borehole data of Kundan et al., (2017) as N7° E in one well and as N40° E in another well drilled in Kachchh-Saurashtra basin (Kundan et al., 2017; Fig. 1). Khadkikar (2002) also reported NE trending SH_{max} from studies on neotectonic joints at SE Saurashtra. Bhonde and Bhatt (2009) confirm the mean NE trend of SH_{max} from the coastline of S Saurashtra. The major stress trends plotted in the offshore region (I) σ_1: N7° E and (II) σ_1: N40° E differs from the stress tensors of the present study area i.e., σ_1: N53° E. The difference in orientation between maximum horizontal stresses (σ_1) of the study area to that to offshore region is (I) N46° E and (II) N13° E. This indicates that from the offshore region into the Rajula area, SH_{max} (corresponds to $\sigma_{1)}$ underwent a rotation.

The T-Tecto software separated the heterogeneous fault-slip data into homogeneous subsets of Phase 1 and Phase 2 deformation events. Phase 2 deformation event, which shows the ~NE-SW trend of SH_{max} (Fig. 4d) is consistent with the results of Gowd and Rao (1992), Khadkikar (2002) and Bhonde and Bhatt (2009). The NE-SW trend of SH_{max} may have prevailed under the transpressive stress regime after the collision of the Indian plate with the Eurasian plate and may have

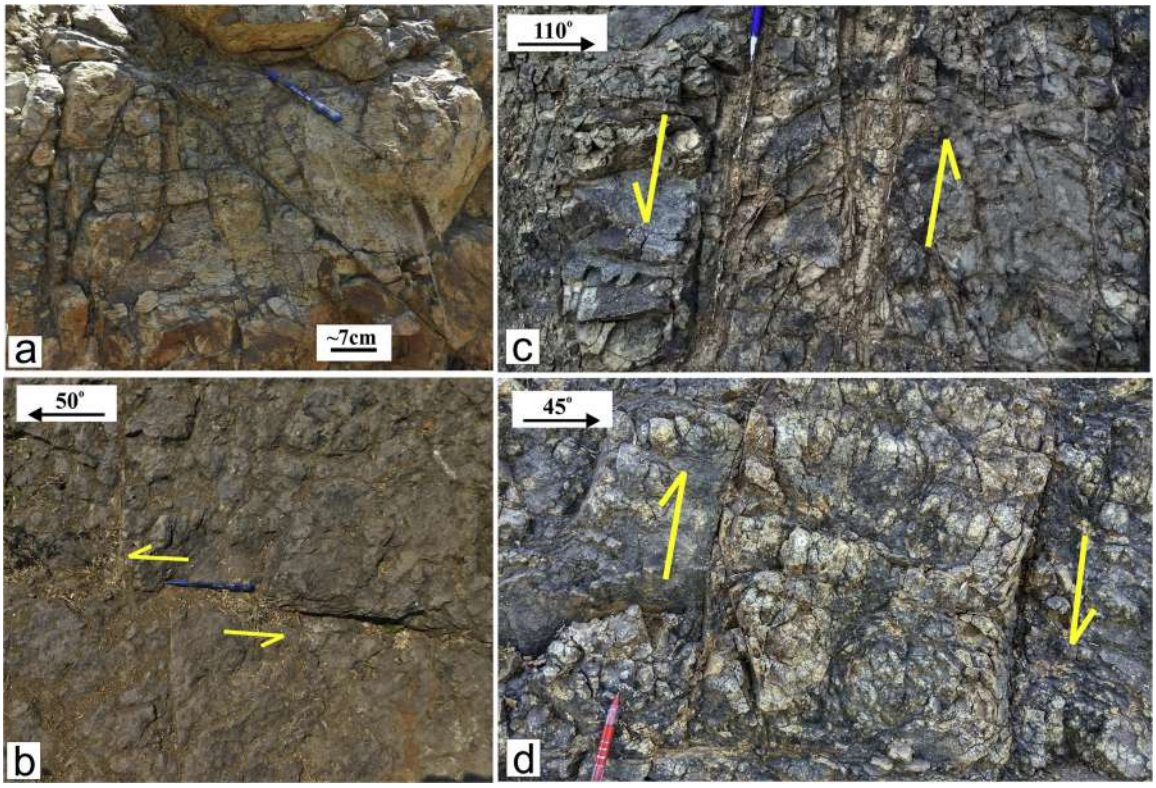

Fig. 5. a) P- and Y-plane (attitude: 330° strike, 35° dip, 240° dip direction) in the highly fractured and sheared basaltic rock on the NW of the "Katar" village (21° 0′ 27″N, 71°19′ 59″E) near Rajula. Slip plane ~ parallels the Katar scarp. (b) Joint plane on trappean flows slipped to ~10 cm by a 50° striking local fault on the Malan river bed near Kantala village (21° 0′ 20″N, 71° 9′ 7″E) observing sub-horizontal exposure. A pen of 14.3 cm as scale. Open tip: slip sense. (c) Slipped vein on a vertical surface observed inside a trench, vertical faulting, near Khadadhar Village (21° 5′ 19″N, 71° 12′ 22″E). Trend of fault: N23°. (d) Wavy P-plane (N93°) and vertical Y-plane (N105°): observed on a vertical surface near Baraftana village (21° 6′ 44.28″N, 71° 29′ 34.17″E), display vertical shear. Part of pen, 10 cm visible, as scale. Y- and P-planes indicating brittle shear.

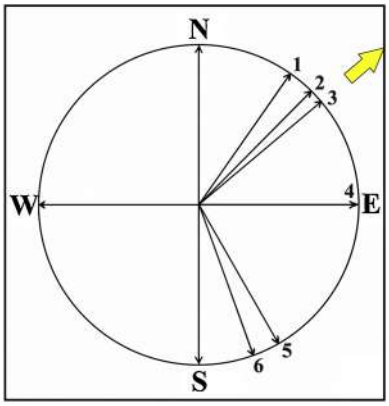

Fig. 6. Summary of brittle slip sense around Katar ridge fault show dominantly a ~NE trending slip. Some data mismatch with the fault trend observed at the Katar ridge. 1. N 35° (Repository Fig. 8a); 2. N 45° (Repository Fig. 8d); 3. N 50° (Fig. 5b); 4. N 90° (Repository Fig. 7a); 5. N 150° (Fig. 5a); 6. N 160° (Repository Fig. 6a).

persisted in Saurashtra till Quaternary as indicated by the work of Bhonde and Bhatt (2009) and Khadkikar (2002) on neotectonic joints found in Quaternary Milliolite deposits in the Saurashtra coastal belt. In the present study, the local deviation in the stress field is exemplified by the NW-SE trend of the phase 1 deformation event (Fig. 4c) which may be due to the local perturbation in the regional stress field. Bhonde and Bhatt (2009) also reported deviation from the NE-SW trend as indicated by NE-SW to E-W and NNE-SSW to NW-SE. Several SH_{max} trends observed in the field suggest complex stress pattern in Saurashtra (Fig. 3h) showing two sets of oblique slip striation trends in a single outcrop generated by multiple deformation events. However, present study suggests that, an overall transpressive stress regime has prevailed that caused the reverse sinistral slip at the Katar Fault.

The results of phase 2 deformation event of Rajula fault slip analysis of the Katar ridge fault using T-Tecto (σ_1 trend: N53° E, plunge: 0°, σ_2 trend: N292° E, plunge: 90°; σ_3 trend N142° E, plunge: 0°) matches also with some of the faults we document from nearby regions (Fig. 6). A few faults do not match with ~ E trend as observed in Katar (Figs. 5b and c, Repository Figs. 8d and e). Deformation sequence in field-scale has so far not been worked out by any structural geologists. The northward movement of the Indian plate probably produced a transpression in the S Saurashtra, such as the Katar region. A strike-slip component of transpression might get predominant at Katar. Transpression involves shortening (thickening) or extension (thinning) component to the steeply dipping or sub-vertical deformation zone favoring lateral extrusion (Dewey et al., 1998; Fossen and Tikoff, 1998) along with uplift/subsidence (Sanderson and Marchini, 1984). The steeply dipping fault plane surface observed on the top of the ridge possibly indicates bulging/thickening by transpression. The Katar Fault is devoid of gouge, breccia and melts. There was no visual effect of shear heating/local metamorphism due to this faulting.

Several lineaments and ridges observed nearby Katar ridge fault trend ~NE, and very rare ~E trending ridges are observed in the surrounding regions. A discontinuous ridge SW of Katar village, W of Nana Barman village, trending ~E has been observed. Our fieldwork revealed that such ridges are devoid of strike-slip faults. At several places, some geomorphic landforms formed due to strike-slip faults such as deflected streams can be noted (Repository Fig. 9).

5.2. Implication for tectonic evolution of SW Saurashtra

The slip characteristics of the Katar Fault provides insight into the tectonic set up of the region around Rajula. Our detailed fault slip analysis clearly suggests oblique slip reverse faulting with sinistral slip to be the dominant deformation style as shown by phase 2 deformation event. The faulting appears to correlate with the phase of tectonic activity after the main extrusive event (Rao, 1971). Oblique faulting with reverse component indicates transpressional stress regime (due to northward movement of Indian plate) along the Katar Fault. The post Deccan trap movement along Katar Fault matches with the east to southeastward tilting of the trappean lava flows occurring around Rajula.

The deformation of the Deccan Trap is not yet understood though structural influences have been emphasized based on dyke patterns. Post-Deccan Trap intrusive activity evidenced by the large Girnar intrusive to the NW of Rajula area caused some syn-intrusive deformation of the basaltic lava flows. The Girnar intrusive has been extensively studied for its petrological and mineralogical characteristics (Mathur et al., 1926; Bose, 1973; Paul et al., 1977). But, the detailed structural studies are not available. However, few radial faults within the intrusive, a circular pattern of faults around the intrusive mass and radial dips of the surrounding trappean lava flows are reported (Mathur et al., 1926; Wellman and McElhinny, 1970). This testifies to the structural deformation of the Deccan Trap lava flows and the stresses induced by the intrusive activity after the Deccan Volcanism. The stresses caused by intrusive activity also caused deformation of dykes as far as Gondal, Savarkundla and Amreli (Mathur et al., 1926; Sethna et al., 2001).

A careful review of the sparse structural information available suggest that the stresses induced by the Girnar intrusive may be much more extensive than documented till now. The swinging of structural grain evidenced by the dyke swarm as EN E-W SW around Rajula possibly resulted due to regional scale stresses caused by the large Girnar intrusive. This suggests that the eastward tilting of the basaltic flows around Rajula also occurred during this phase. Our field observation during the present study shows that the E-W trending Katar Fault cuts across the NE-SW strike of the dyke swarm around Rajula. The fault also offsets the NE-SW trending ridge consisting of eastward tilted trappean flows at Katar village. We therefore attribute the faulting along Katar Fault to transpressive phase of tectonic activity after the swinging of the dyke swarm and tilting of the trappean flows.

The tectonic evolution and the shape of the Saurashtra peninsula is linked to the regional events of breakup of the western margin of Indian plate as it separated from the Gondwanaland and rapidly drifted northward to collide with the Eurasian plate spanning a total period of approximately 160 My (Chatterjee and Bajpai, 2016). The motion of the Indian plate was most rapid (up to 20 cm/yr) during the 67-52 Ma time period (Mckenzie and Sclater, 1971; Yoshida and Hamano, 2015; Chatterjee and Bajpai, 2016), which encompasses the events of Deccan volcanism, separation of Seychelles (~ 64 Ma), initiation of spreading at Carlsberg ridge at ~ 63.4 Ma (Collier et al., 2008; van Hinsbergen et al., 2011) and post trappean intrusive activity in Saurashtra. The rapid movement of the plate has been linked to the acceleration provided by the rise of Reunion plume which is also responsible for the Deccan Volcanism, thinning of crust, slab pull and/or ridge push (Collier et al., 2008; Cande and Stegman, 2011). Also, the Indian plate was ~ 1000 km away from the Reunion plume at the time of separation of Seychelles (Chatterjee and Bajpai, 2016). Onset of India-Asia collision at ~ 55 Ma gradually slowed down the motion to 5 cm/year by ~ 52 Ma (Chatterjee and Bajpai, 2016).

As discussed above, the continental margin of Saurashtra suffered significant tectonic activity during the northward drift of the Indian plate. However, the transpressional stress regime occurred only during the collision of the Indian plate and the Eurasian plate and enduring till date in the far north (Chatterjee and Bajpai, 2016). The formation of the Katar Fault and its further reactivation under transpression is suggested by our fault slip analysis. In view of this, we infer that the E-W trending Katar Fault was formed due to the onset of compression induced by the collision of the Indian plate. We suggest that the transpression could have been facilitated by the syn-collisional rotation of the Indian plate (Biswas, 1982). Moreover, the E-W orientation of the Katar Fault, perpendicular to the northward directed compression is favorable for transpression induced tectonic activity along the fault.

The Katar Fault presumably reactivated multiple times as the same stress scenario continued to exist through most part of the Cenozoic as the Indian plate pushed northward due to the spreading of the Carlsberg ridge. We believe that this is a distinct possibility as the highly fragmented western continental margin of India comprises of several faults, which were reactivated multiple times during the Cenozoic (Biswas, 1987; Merh, 1995; Maurya, 2000; Maurya et al., 2017). Our field studies further eastward along the trend of the Katar Fault also revealed evidence of tectonic reactivation. The thin band of Miocene rocks (Gaj Formation) fringing the Deccan trap shows southward dip along the inferred eastward trace of the fault, pointing to a post-Miocene phase of reactivation. The outcrops of the Middle Pleistocene – Holocene miliolite deposits are also limited to ~ 5 km south of the fault line. Significantly, the miliolites show two raised notches dated to ~ 125 ka BP and 6 ka BP, along the coastline of Jafarabad (~ 16 km S of the study area) which suggests 7 m coastal margin uplift after correcting for the sea level fluctuation since ~125 Ka (Juyal et al., 1995). The eastward trace of the Katar Fault correlates with the straight E-W trending margin of a landward indentation of the coastline. The recent mudflats abruptly terminate along the line indicating influence on the coastal geomorphology. This together with recent earthquake swarm activity to the north and west of Rajula suggests neotectonically active environment in and around the immediate vicinity of the Katar Fault. A further detailed tectonic study is warranted to fully comprehend the deformation of Deccan traps in compressional stress regime in Saurashtra and to unambiguously link the Katar Fault and other faults to neotectonic and landscape evolution of the area.

6. Conclusions

The present study has led to the following conclusions.

1 A previously unmapped fault, the E-W trending Katar Fault is investigated from SW Saurashtra which cuts across the NE-SW trending dyke swarm and the strike of the southeastward tilted Deccan Trap lava flows.
2 Detailed fault slip analyses indicates that the Katar Fault is an oblique slip reverse fault with sinistral slip. The analyses suggests two phases of reactivations under transpressional stress regime. Our paleostress analysis results of phase 2 deformation event is σ_1 trend: N53° E, plunge: 0°, σ_2 trend: N292° E, plunge: 90°; σ_3 trend N142° E, plunge: 0°. The difference in SH_{max} trend of the offshore region to that of the present study area shows rotation by 46° and 13° after the main eruptive phase of Deccan Trap.
3 We infer that the Katar Fault developed under transpresssional stress regime induced by the collision and anti-clockwise rotation of the Indian plate and post-dates the swing of the dyke swarm from EN E-W SW in the east to NE-SW trend in the area around Rajula. The swing of the trend of the dyke swarm and eastward tilt of the trappean lava flows are tentatively attributed to the stresses induced by the large Girnar intrusive body in the NW immediately after the Deccan volcanic activity.
4 The Katar Fault shows evidence of further multiple reactivations including in post-Miocene and Quaternary times suggesting continuation of transpressional stress regime. The present study emphasizes the need for further similar studies to delineate the fault pattern and structural deformation of the Deccan Traps in Saurashtra to understand the neotectonic evolution and recurrent earthquake swarm activity.

Acknowledgements

The present study was funded from a Ministry of Earth Sciences' (India) research project number MoES/P.O.(Seismo)/1(170)/2013 to DMM. A research sabbatical for the year 2017 and a research grant provided by IIT Bombay to S. Mukherjee is thankfully acknowledged. Akash Padmalal and Prabhuti Tiwari provided assistance in field studies. Thorough critical and positive review comments from two anonymous reviewers and efficient editorial handling by Volker Klemann (J Geodyn) are gratefully acknowledged.

Appendix A

T-Tecto

It utilizes the Gauss method to sort out the heterogeneous fault slip data into the homogeneous fault subsystems (Zalohar and Vrabec, 2007) and the Right Dihedra Method (RDM) (Angelier, 1989, 1990) to calculate the stress tensor. The RDM is based on the Anderson's theory of faulting. The orientation of the maximum principal stress axis (σ_1) is constrained to the (pressure) P-quadrant, while orientation of the minimum principal stress axis (σ_3) is constrained to the tension (T) quadrant associated with a chosen fault. P- and T- quadrants are defined by orientation and slip sense of the fault planes. Considering that faults active in the same stress field have a common intersection of the P- and the T- quadrants enables constraining ~ direction of the principal stresses. The RDM applies on the homogeneous subsystems of faults. The Gauss method is based on fault-slip data inversion, which involves the concept of the best-fit stress tensor. T-Tecto identifies faults compatible with the stress tensor with a threshold angular misfit (Zalohar and Vrabec, 2007).

Win-Tensor (v5.8.7)

The fault data are plotted in the Schmidt equal area projection. The stress tensor is computed using RDM for the total data set. Fault data that best fits the result is then sorted out. Inversion result of the fault slip data are presented as a projection. The software obeys Bott's (1959) assumption that a plane slips towards the maximum resolved shear stress. Compressional and extensional quadrants are deduced as per the orientation of the fault plane, the slip line and the sense of movement. Detail in Delvaux and Sperner (2003).

Faultkin (v 7.7.2)

It graphically constructs the principal axes of extension and shortening for the input fault-slip data (Marrett and Allmendinger, 1990; Allmendinger et al., 2012). It uses the dynamic "P & T Dihedra Method" and the kinematic "P" (shortening) and "T" (extension) axes. The kinematic axes are displayed either as scatter plot or as contours. The direction of the principal stress axes can be calculated using linked Bingham distribution statistics function. Detail in Angelier and Mechler, (1977) and Angelier (1990).

Appendix B. Supplementary data

Supplementary material related to this article can be found, in the online version, at doi:https://doi.org/10.1016/j.jog.2018.06.004.

References

Allmendinger, R.W., Cardozo, N., Fisher, D., 2012. Structural Geology Algorithms: Vectors and Tensors in Structural Geology. Cambridge University Press.
Angelier, J.T., Mechler, P., 1977. Sur une methode graphique de recherche des contraintes principales egalement utilisables en tectonique et en seismologie: la methode des diedres droits. Bull. Soc. Géol. Fr. 7 (6), 1309–1318.
Angelier, J., 1989. From orientation to magnitudes in paleostress determinations using fault slip data. J. Struct. Geol. 11, 37–50.
Angelier, J., 1990. Inversion of field data in fault tectonics to obtain the regional stress. A new rapid direct inversion method by analytical means. Geophys. J. Int. 103, 363–376.
Bastia, R., Radhakrishna, M., 2012. Basin evolution and petroleum perspectivity of the continental margins of India. 1st edition. Dev. Petroleum Sci. 59 Oxford, UK.
Betka, P., Klepeis, K., Mosher, S., 2016. Fault kinematics of the Magallanes-Fagnano fault system, southern Chile; an example of diffuse strain and sinistral transtension along a continental transform margin. J. Struct. Geol. 85, 130–153.
Bhatt, N., Patidar, A.K., Maurya, D.M., Chamyal, L.S., 2006. Delineation of three shallow subsurface faults using GPR in south Saurashtra, western India. In: 11th International Conference on Ground Penetrating Radar. Columbus Ohio, USA.
Bhattacharya, G.C., Subramanyam, V., 1986. Extension of the Narmada-Son Lineament on the continental margin off Saurashtra, Western India as obtained from magnetic measurements. Mar. Geophys. Res. 8, 329–344.
Bhattacharya, S.N., Karanth, R.V., Dattatrayam, R.S., Sohoni, P.S., 2004. Earthquake sequence in and around Bhavnagar, Saurashtra, western India during August–December 2000 and associated tectonic features. Curr. Sci. India 1165–1170.
Bhonde, U., Bhatt, N., 2009. Joints as fingerprints of stress in the quaternary carbonate deposits along coastal Saurashtra, Western India. J. Geol. Soc. Ind. 74, 703–710.
Biswas, S.K., 1982. Rift basins in western margin of India and their hydrocarbon prospects with special reference to Kutch basin. AAPG Bull. 66 (10), 1497–1513.
Biswas, S.K., 1987. Regional tectonic framework, structure and evolution of the western margin basins of India. Tectonophysics 135, 307–327.Bose, M. K., 1973. Petrology and geochemistry of the igneous complex of Mount Girnar, Gujarat, India. Contrib. Miner. Petrol. 39 (3), 247–266.
Bose, M.K., 1973. Petrology and geochemistry of the igneous complex of Mount Girnar, Gujarat, India. Contrib. Miner. Petrol. 39 (3), 247–266.
Bott, M.H.P., 1959. The mechanism of oblique-slip faulting. Geol. Mag. 96, 109–117.
Cande, S.C., Stegman, D.R., 2011. Indian and African plate motions driven by the push force of the Reunion plume head. Nature 475 (7354), 47.
Chamyal, L.S., Maurya, D.M., Bhandari, S., Rachna, R., 2002. Late Quaternary geomorphic evolution of the lower Narmada Valley, western India: implications for neotectonic activity along the Narmada–Son Fault. Geomorphology 46, 177–202.
Chandrasekhar, D.V., Mishra, D.C., Rao, G.P., Rao, J.M., 2002. Gravity and magnetic signatures of volcanic plugs related to Deccan volcanism in Saurashtra, India and their physical and geochemical properties. Earth Planet. Sci. Lett. 201 (2), 277–292.
Chatterjee, S., Bajpai, S., 2016. India's northward drift from Gondwana to Asia during the late cretaceous-eocene. In Proc. Indian Natl. Sci. Acad. 82 (3), 479–487.
Chatterjee, N., Bhattacharji, S., 2001. Origin of the felsic dikes and basaltic dikes and flows in the Rajula-Palitana-Sihor area of the Deccan Traps, Saurashtra, India: a geochemical and geochronological study. Int. Geol. Rev. 43, 1094–1116.
Chatterjee, N., Bhattacharji, S., 2004. A preliminary geochemical study of zircons and monazites from Deccan felsic dikes, Rajula, Gujarat, India: Implications for crustal melting. Proc. Ind. Acad. Sci. 113, 533–542.
Collier, J.S., Sansom, V., Ishizuka, O., Taylor, R.N., Minshull, T.A., Whitmarsh, R.B., 2008. Age of Seychelles–India break-up. Earth Planet. Sci. Lett. 272 (1-2), 264–277.
Dasgupta, S., Mukherjee, S., 2017. Brittle shear tectonics in a narrow continental rift: asymmetric non-volcanic Barmer basin (Rajasthan, India). J. Geol. 125, 561–591.
Dasgupta, S., Pande, P., Ganguli, D., Iqbal, Z., Sanyal, K., Venkatraman, N.V., Dasgupta, S., Sural, B., Harendranath, L., Mazumdar, K., Sanyal, S., Roy, A., Das, L.K., Misra, P.S., Gupta, H., et al., 2000. Kutch and Saurashtra area of Gujarat. In: Narula, P.L., Acharyya, S.K., Banerjee, J. (Eds.), Seismotectonic Atlas of India and its Environs. Geol. Surv. Ind. Calcutta p. 39. SEISAT 18.
Dasgupta, S., 2018. Remote sensing in lineament identification: examples from western India. In: Fagereng, A., Billi, A. (Eds.), Problems and Solutions in Structural Geology. Developments in Structural Geology and Tectonics, Series Editor: S. Mukherjee. Elsevier.
Delvaux, D., Moeys, R., Stapel, G., Petite, C., Levi, K., Miroshnichenko, A., Ruzhich, V., San'kov, V., 1997. Paleostress reconstructions and geodynamics of the Baikal region, Central Asia, Part 2. Cenozoic rifting. Tectonophysics 282, 1–38.
Delvaux, D., Sperner, B., 2003. Stress tensor inversion from fault kinematic indicators and focal mechanism data: the TENSOR program. In: In: Nieuwland Ed, D. (Ed.), New Insights into Structural Interpretation and Modelling 212. Geol. Soc., London, Spec. Publ., pp. 75–100.
Dewey, J.F., Holdsworth, R.E., Strachan, R.A., 1998. Transpression and Transtension Zones 135. Geol. Soc., London, Spec. Publ., pp. 1–14.
DGH Directorate General of Hydrocarbon (Accessed on 29-Aug-2017). http://dghindia.gov.in/assets/downloads/56ceb7d978aSaurashtra_Basin_20.pdf.
Doblas, M., 1998. Slickenside kinematic indicators. Tectonophysics 295, 187–197.
Doblas, M., Mahecha, V., Hoyos, M., 1997. Slickenside and fault surface kinematic indicators on active normal faults of the Alpine Betic cordilleras, Granada, southern Spain. J. Struct. Geol. 19, 159–170.
Fossen, H., 2016. Structural Geology. Cambridge University Press.
Fossen, H., Tikoff, B., 1998. Extended models of transpression and transtension, and application to tectonic settings. Geol. Soc., Lond., Spec. Publ. 135, 15–33.
Gowd, T.N., Rao, S.V., 1992. Tectonic stress field in the Indian subcontinent. J. Geophys. Res. 97, 11879–11888.
Gowd, T.N., Srirama Rao, S.V., Chary, K.B., 1996. Stress field and seismicity in the Indian shield: effects of the collision between Indian and Eurasia. In: In: Ren, W.R., Aki, K. (Eds.), Mechanics Problems in Geodynamics Part II. BirkhauserVerlag, Basel; Boston; Berline 146. pp. 503–531.
Joshi, P.N., Maurya, D.M., Chamyal, L.S., 2013. Morphotectonic segmentation and spatial variability of neotectonic activity along the Narmada–Son Fault, Western India: remote sensing and GIS analysis. Geomorphol 180–181, 292–306.
Juyal, N., Pant, R.K., Bhushan, R., Somyajulu, B.L.K., 1995. Radiometric dating of Late

Quaternary sea levels of the Saurashtra coast, western India: an experiment with Oyster and Clam shells. Memmoir Geol. Soc. India 32, 372–379.
Kaymakci, N., 2006. Kinematic development and paleostress analysis of the Denizli Basin (Western Turkey): implications of spatial variation of relative paleostress magnitudes and orientations. J. Asian Earth Sci. 27, 207–222.
Khadkikar, A.S., 2002. Late Quaternary neotectonic joints: confirmation of the connection between jointing and contemporary tectonic stress. Geophys. Res. Lett. 29, 1029–2002.
Kounov, A., Burg, J.P., Bernoulli, D., Seward, D., Ivanov, Z., Dimov, D., Gerdjikov, I., 2011. Paleostress analysis of Cenozoic faulting in the Kraishte area, SW Bulgaria. J. Struct. Geol. 33 (5), 859–874.
Kundan, A., Desai, A., Bahuguna, S., Talreja, R., Nakhle, A., Zayyan, M., Narayanan, S., Tewari, P., Purohit, S., Basu, J., 2017. Revolutionary drilling performance in challenging HPHT and basaltic environment of Kutch and Saurashtra exploration field. Soc. Petr. Eng. Conf.
Mahadevan, T.M., 1994. Deep continental structure of India: a review: Bangalore. Geol. Soc. Ind. Mem. 28, 242.
Marrett, R.A., Allmendinger, R.W., 1990. Kinematic analysis of fault-slip data. J. Struct. Geol. 12, 973–986.
Mathur, K.K., Dubey, V.S., Sharma, N.L., 1926. Magmatic differentiation in Mount Girnar. J. Geol. 34 (4), 289–307.
Maurya, D.M., 2000. History of tectonic evolution of Gujarat alluvial plains, western India during quaternary: a review. J. Geol. Soc. Ind. 55, 343–366.
Maurya, D.M., 2017. A review and new data on neotectonic evolution of active faults in Kachchh basin, Western India: legacy of post-deccan trap tectonic inversion. In: Mukherjee, S., Misra, A.A., Calve's, G., Nemcok, M. (Eds.), Tectonics of Deccan Large Igneous Province, 445. Geological Society of London Special Publication, London, pp. 237–268.
McKenzie, D., Sclater, J.G., 1971. The evolution of the Indian Ocean since the Late Cretaceous. Geophys. J. Int. 24 (5), 437–528.
Means, W.D., 1987. A newly recognized type of slickenside striations. J. Struct. Geol. 9, 585–590.
Merh, S.S., 1995. Geology of Gujarat. Geol. Soc. Ind. Bangalore 106–130.
Mishra, K.S., 2008. Dyke swarms and Dykes within the Deccan Volcanic Province, India. In: Srivastava, R.K., ShivajiCh, Rao NVC (Eds.), Indian Dykes: Geochemistry, Geophysics and Geochronology. Narosa Publishing House, Delhi pp. 57-72.
Misra, A.A., Mukherjee, S., 2017. Dyke-brittle shear relationships in the Western Deccan Strike-slip Zone around Mumbai (Maharashtra, India). In: In: Mukherjee, S., Misra, A.A., Calvès, G., Nemčok, M. (Eds.), Tectonics of the Deccan Large Igneous Province 445. Geol. Soc., London, Spec. Publ, pp. 269–295.
Misra, A.A., Bhattacharya, G., Mukherjee, S., Bose, N., 2014. Near N-S paleo-extension in the western Deccan region in India: Does it link strike-slip tectonics with India-Seychelles rifting? Int. J. Earth Sci. 103, 1645–1680.
Misra, A.A., Sinha, N., Mukherjee, S., 2015. Repeat ridge jumps and microcontinent separation: insights from NE Arabian Sea. Marine Petroleum Geology. 59, 406–428.
Mukherjee, S., 2013. Higher Himalaya in the Bhagirathi section (NW Himalaya, India): its structures, backthrusts and extrusion mechanism by both channel flow and critical taper mechanisms. Int. J. Earth Sci. 102, 1851–1870.
Mukherjee, S., 2014. Atlas of Shear Zone Structures in Meso-Scale. Springer Geology, Cham, pp. 1–124.
Mukherjee, S., 2015a. A review on out-of-sequence deformation in the Himalaya. In: In: Mukherjee, S., Carosi, R., van der Beek, P., Mukherjee, B.K., Robinson, D. (Eds.), Tectonics of the Himalaya Geological Society 412. Special Publications, London, pp. 67–109.
Mukherjee, S., 2015b. Atlas of Structural Geology. Elsevier, Amsterdam p. 39. SEISAT 18420152-1.
Mukherjee, S., Koyi, H.A., 2010. Higher Himalayan Shear Zone, Sutlej Section- structural geology & extrusion mechanism by various combinations of simple Shear, pure shear & channel flow in shifting modes. Int. J. Earth Sci. 99, 1267–1303.
Pandey, J.P., Singh, K.R.K., Singh, M., Kalaiarasan, T., Mukherjee, R.N., Marathe, U.G., 2013. Late oligocene sandstone reservoirs of Saurashtra offshore, significance of their deposition – an integrated study resulting in regional clastic model. In: 10th Biennial International Conference & Exposition. Kochi. India.
Paul, D.K., Potts, P.J., Rex, D.C., Beckinsale, R.D., 1977. Geochemical and petrogenetic study of the Girnar igneous complex, Deccan volcanic province, India. Geol. Soc. Am. Bull. 88 (2), 227–234.
Ramasamy, S.M., 1995. Deformation tectonics of Deccan volcanics of Southern Saurashtra, India and its relation to western extension of Narmada Lineament. In: Srivastava, R.K., Chandra, R. (Eds.), Magmatism in Relation to Diverse Tectonic Settings. A. A. Balkema, Rotterdam, pp. 195–208.
Rao, S.S., 1971. Minor intrusions towards the east of the Girnar hills. Bull. Volcanologique 35, 975.
Rastogi, B.K., Kumar, S., Aggrawal, S.K., Mohan, K., Rao, N., Rao, N.P., Kothyari, G.C., 2013. The October 20, 2011 M_w 5.1 Talala earthquake in the stable continental region of India. Nat. Hazard. 65, 1197–1216.
Reddy, P.R., 2005. Crustal velocity structure of western India and its use in understanding intraplate seismicity. Curr. Sci. 88, 1652–1657.
Sanderson, D.J., Marchini, W.R.D., 1984. Transpression J. Struct. Geol. 6, 449–458.
Sethna, S.F., Sethna, B.S., Kothare, P., Rao, D.R.K., Saraf, P.D., Venkateshwarlu, M., Patil, S.K., 2001. A note on palaeomagnetic evidence to show tectonic deformation in the Deccan Volcanic Province of Saurashtra, Western India. Curr. Sci. India 1067–1069.
Simón, J. L., (In press) Forty years of paleostress analysis: has it attained maturity?. Struct. Geol. Elsevier, nd.
Valdiya, K.S., 2016. The Making of India, 2nd edition. Springer. Bengaluru.
van Gent, H.W., Back, S., Urai, J.L., Kukla, P.A., Reicherter, K., 2009. Paleostresses of the Groningen area, the Netherlands—results of a seismic based structural reconstruction. Tectonophysics 470, 147–161.
van Hinsbergen, D.J., Steinberger, B., Doubrovine, P.V., Gassmöller, R., 2011. Acceleration and deceleration of India-Asia convergence since the Cretaceous: roles of mantle plumes and continental collision. J. Geophys. Res.: Solid Earth (B6), 116.
Varadarajan, K., Ganju, J.L., 1989. Regional geophysical lineaments their tectonic and economic significance: Bangalore. Geol. Soc. Ind. Mem. 12, 242.
Verma, R.K., Mittal, G.S., 1972. Palaeomagnetism of a vertical sequence of traps from Mount Girnar, Gujrat, India. Geophys. J. Int. 29 (3), 275–287.
Wallace, R.E., 1951. Geometry of shearing stress and relation to faulting. J. Geol. 59 (2), 118–130.
Wellman, P., McElhinny, M.W., 1970. K–Ar age of the Deccan traps, India. Nature 227 (5258), 595–596.
Yadav, R.B., Tripathi, J.N., Rastogi, B.K., Chopra, S., 2008. Probabilistic assessment of earthquake hazard in Gujarat and adjoining region of India. Pure Appl. Geophys. 165, 1813–1833.
Yadav, R.B.S., Papadimitriou, E.E., Karakostas, V.G., Shanker, D., Rastogi, B.K., Chopra, S., Singh, A.P., Kumar, S., 2011. The 2007 Talala, Saurashtra, western India earthquake sequence: tectonic implications and seismicity triggering. J. Asian Earth Sci. 40, 303–314.
Yoshida, M., Hamano, Y., 2015. Pangea breakup and northward drift of the Indian subcontinent reproduced by a numerical model of mantle convection. Sci. Rep. 5, 8407.
Zalohar, J., 2018. The Omega-Theory: A New Physics of Earthquakes. In: In: Mukherjee, S. (Ed.), Developments in Structural Geology and Tectonics Vol. 2. Elsevier, Amsterdam, pp. 1–558 ISBN: 978-0-12-814580-7.
Zalohar, J., Vrabec, M., 2007. Paleostress analysis of heterogeneous fault-slip data: the Gauss method. J. Struct. Geol. 29, 1798–1810.